Earth and Planetary Science Letters 505 (2019) 30–41

Contents lists available at ScienceDirect

Earth and Planetary Science Letters

www.elsevier.com/locate/epsl

The roles of climate and human land-use in the late Holocene rainforest crisis of Central Africa

Germain Bayon [a,b,*], Enno Schefuß [c], Lydie Dupont [c], Alberto V. Borges [d], Bernard Dennielou [a], Thibault Lambert [e], Gesine Mollenhauer [f], Laurence Monin [b], Emmanuel Ponzevera [a], Charlotte Skonieczny [a,g], Luc André [b]

[a] IFREMER, Marine Geosciences Unit, F-29280 Plouzané, France
[b] Royal Museum for Central Africa, Department of Earth Sciences, B-3080 Tervuren, Belgium
[c] MARUM – Center for Marine Environmental Sciences, Bremen University, D-28359 Bremen, Germany
[d] Chemical Oceanography Unit, Université de Liège, B-4000, Belgium
[e] Institute of Earth Surface Dynamics, University of Lausanne, CH-1015, Switzerland
[f] Alfred Wegener Institute for Polar and Marine Research, D-27570 Bremerhaven, Germany
[g] Laboratoire Geosciences Paris-Sud, UMR CNRS 8148, Université de Paris-Sud, Université Paris-Saclay, F-91405 Orsay, France

ARTICLE INFO

Article history:
Received 15 June 2018
Received in revised form 12 October 2018
Accepted 14 October 2018
Available online xxxx
Editor: D. Vance

Keywords:
neodymium isotopes
suspended particulates
Congo Basin
ENSO
human land-use
deforestation

ABSTRACT

There is increasing evidence that abrupt vegetation shifts and large-scale erosive phases occurred in Central Africa during the third millennium before present. Debate exists as to whether these events were caused by climate change and/or intensifying human activities related to the Bantu expansion. In this study, we report on a multi-proxy investigation of a sediment core (KZR-23) recovered from the Congo submarine canyon. Our aim was to reconstruct climate, erosion and vegetation patterns in the Congo Basin for the last 10,000 yrs, with a particular emphasis on the late Holocene period. Samples of modern riverine suspended particulates were also analyzed to characterize sediment source geochemical signatures from across the Congo watershed. We find that a sudden increase of bulk sediment aluminium-to-potassium (Al/K) ratios and initial radiocarbon ages of bulk organic matter occurred after 2,200 yrs ago, coincident with a pollen-inferred vegetation change suggesting forest retreat and development of savannas. Although hydrogen isotope compositions of plant waxes (δD_{wax}) do not reveal a substantial hydroclimate shift during this period, neodymium isotopes and rare earth elements in detrital fractions indicate provenance changes for the sediment exported from the Congo Basin at that time, hence suggesting a reorganization of spatial rainfall patterns across Central Africa during this event. Taken together, these findings provide evidence for changing landscapes in Central Africa from about 2,200 yrs ago, associated with synchronous events of vegetation changes and enhanced erosion of pre-aged and highly weathered soils. These events coincided remarkably well with the arrival of Iron Age communities into the rainforest, as inferred from comparison to regional archaeological syntheses. While the human impact on the environment remains difficult to quantify at the scale of the vast Congo Basin, we tentatively propose that strengthening of El Niño-Southern Oscillation (ENSO) variability at that time played a key role in triggering the observed environmental changes, and possibly acted as a driver for the eastward migration of Bantu-speaking peoples across Central Africa.

1. Introduction

About 5,000 yrs ago, early farmers originating from West Africa started to migrate southward, leading within a few thousand years to widespread diffusion of Bantu languages and cultural innovations across sub-Saharan Africa (Diamond and Bellwood, 2003; Phillipson, 2005). The Bantu migrations occurred at a time when landscapes were adjusting to a drier climate (Bostoen et al., 2015). At ca. 4,000 and 2,500 yr before present (BP), forest cover declined significantly at the periphery and core of the central African rainforest, respectively (Vincens et al., 1998; Maley, 2002; Ngomanda et al., 2009; Bostoen et al., 2015; Maley et al., 2018), probably facilitating the migration of Bantu-speaking peoples through opening of savanna corridors (Grollemund et al., 2015). Abundant evidence for intense sediment reworking and strong erosion is recorded at this time in soil sequences from the central African rainforest

* Corresponding author at: IFREMER, Marine Geosciences Unit, F-29280 Plouzané, France.
E-mail address: gbayon@ifremer.fr (G. Bayon).

https://doi.org/10.1016/j.epsl.2018.10.016
0012-821X/

(Thiéblemont et al., 2013, 2014; Maley et al., 2018). It is generally assumed that both vegetation shifts and erosive phases were related to climate change (Lézine et al., 2013; Bostoen et al., 2015; Maley et al., 2018). However, debate exists as to whether these events could have partly resulted from the development of agriculture and iron smelting technology amongst the Bantu populations (Willis et al., 2004; Bayon et al., 2012; Maley et al., 2012; Neumann et al., 2012). Using various geochemical proxies, Bayon et al. (2012) identified a pulse of intense weathering in late Holocene sediments deposited at the Congo deep-sea fan, which they attributed to increasing land-use coinciding with the settlement of Iron Age agriculturalists in Central Africa. More recently, a study conducted at Lake Barombi (Cameroon) also reported new evidence for an abrupt deforestation event in Western Central Africa about 2,600 yrs ago, which was interpreted, in absence of any particular hydrological change, as the consequence of human activities (Garcin et al., 2018). Were humans or climate, or a combination of both factors, responsible for the rainforest crisis and intense erosional events? This question remains open, mostly due to a lack of knowledge regarding the environmental history of the Congo Basin during the last few thousand years, as exemplified by the recent discovery of a much larger than expected peatland complex of Holocene age in its central region (Dargie et al., 2017). Rainfall patterns in tropical Africa are complex and subject to various influences associated with latitudinal variations of the tropical rainbelt and zonal east–west gradients driven by Atlantic and Indian Ocean sea-surface temperatures (Singarayer and Burrough, 2015). To date, no coherent framework exists for the interpretation of late Holocene palaeoenvironmental records in this vast region.

To detect past natural climate variability and potential anthropogenic influence in Central Africa, we analyzed sediment core KZR-23 recovered from the active submarine canyon of the Congo River (Fig. 1). The Congo submarine canyon incising into the mouth acts as a direct source-to-sink route for sediments from the Congo River watershed to the deep-sea (Babonneau et al., 2004). Consequently, sedimentation rates recorded for core KZR-23 are much higher (about 170 cm/kyr) compared to those of other nearby marine sites (about 10 cm/kyr) investigated so far (Schefuß et al., 2005; Bayon et al., 2012). It therefore provides a continuous and unique high-resolution record of sediment export and environmental changes in the Congo Basin for the Holocene period. In this study, we report findings from a combined application of tracers for chemical weathering intensity (aluminium-to-potassium), soil erosion (soil-derived lipids and radiocarbon analyses of bulk sediment organic matter), sediment provenance (neodymium isotopes and rare earth elements), precipitation (hydrogen isotope composition of leaf waxes), and vegetation change (pollen).

2. Materials and methods

2.1. The Congo Basin: climate, geological setting and land cover patterns

The Congo River Basin is the largest African river system, covering an area of about $3.8 \cdot 10^6$ km^2 that ranges across the equator from about 9°N to 14°S. Its source is in the south-eastern part of the Democratic Republic of Congo; a region drained by the Upper Congo (or Lualaba) and partly fed by some of the large lakes of the East African Rift Valley, such as Lake Tanganyika and Lake Kivu. The Congo River then flows northward and later westward towards a large depression referred to as the 'Cuvette Centrale', covered by equatorial rainforest and floodplains (Fig. 1A). This depression accounts for almost 50% of the catchment area of the Congo River, hosts an extended peatland complex (Dargie et al., 2017) and is a large source of greenhouse gases to the atmosphere (Borges et al., 2015). It is characterized by a low mean slope (<2 cm/km), low flow velocities (Laraque et al., 2013), and is joined by the Oubangui, the largest right-bank tributary, which drains the northern part of the Congo Basin. Then, the Congo River moves south-westward and is joined by the Kasai River, the ma-

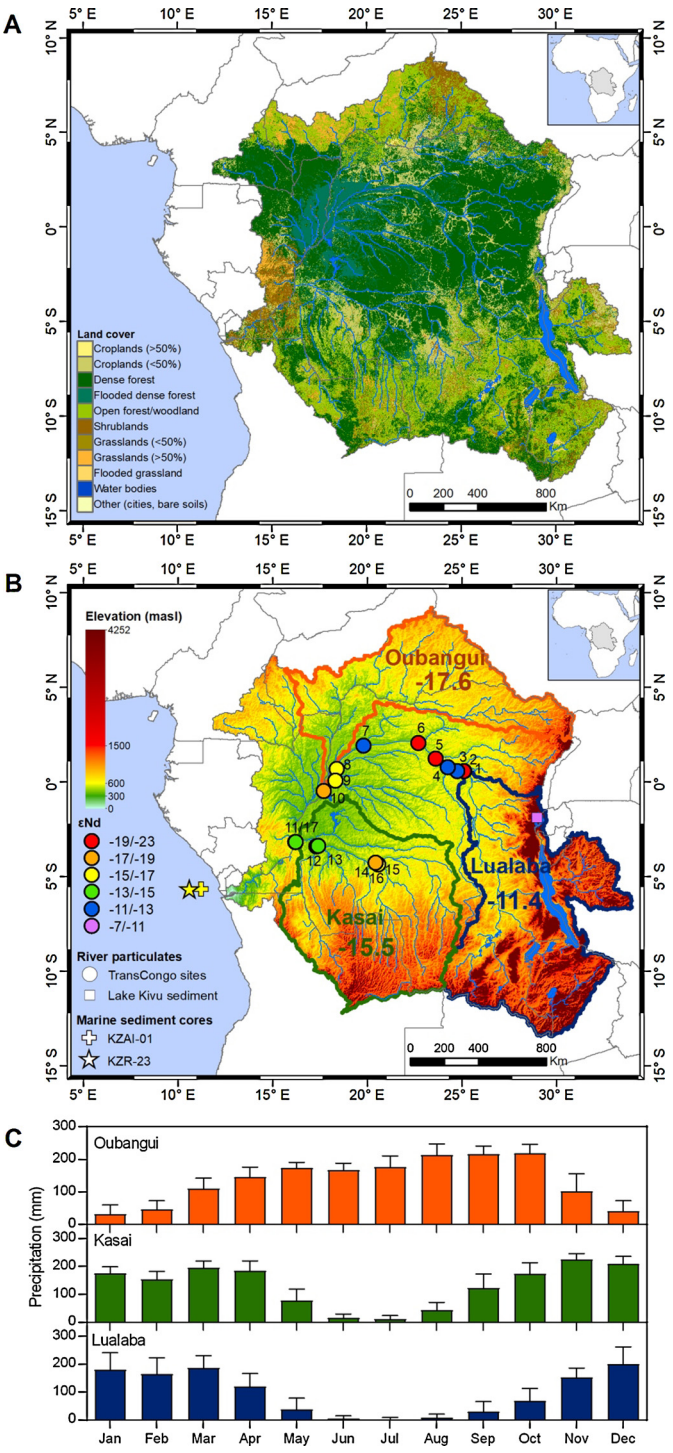

Fig. 1. Study area and location of marine sediment core KZR-23. (A) Land cover and vegetation patterns in the Congo Basin (from Lambert et al., 2016). (B) Map of the Congo River Basin and main tributaries, with position of the suspended river particulates investigated during earlier work (Allègre et al., 1996; squares) and this study (TransCongo samples: circles). The range of neodymium isotopic compositions (ε_{Nd}) for suspended particulates is denoted top right. (C) Rainfall charts for average monthly precipitations (mm) in the Oubangui, Kasai and Upper Congo (Lualaba) sub-basins of the Congo River Basin. Rainfall data from the CLIMWAT climatic database managed by the Food and Agriculture Organization of the United Nations (FAO).

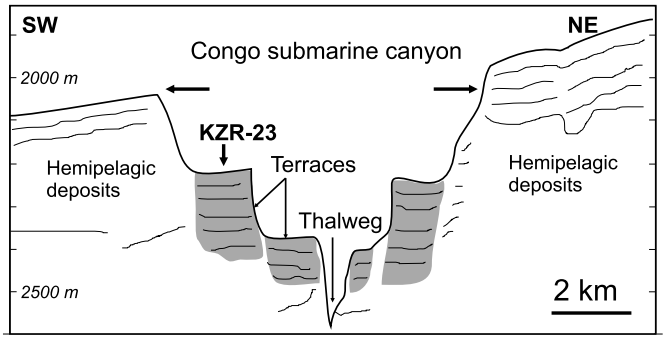

Fig. 2. Schematic position of core KZR-23 in the Congo submarine canyon. Modified from Babonneau et al. (2004).

jor left-bank tributary, originating from the high-plateaus in the southern part of the watershed.

Distinct physiographic regions compose the Congo Basin. The Cuvette Centrale is characterized by an equatorial climate, while the marginal regions of the Congo Basin all display tropical climatic conditions with pronounced seasonal rainfall variability (Fig. 1C). The northern part of the basin (drained by the Oubangui River) receives most rainfall from March to October when the rainbelt migrates to its northern position. In contrast, the southern and eastern parts of the watershed (drained by the Kasai and the Lualaba rivers) mainly receive precipitation from September to April when the rainbelt moves south (Fig. 1C). In terms of geological setting, the northern and eastern parts of the Congo Basin are dominated by Archaean and Proterozoic metamorphic basement rocks, while the southwestern part of the watershed is mostly composed of Mesozoic and Cenozoic sedimentary rocks (Bayon et al., 2018). Neogene volcanic rocks associated with the East African Rift system are also encountered in the eastern part of the basin.

2.2. Core KZR-23 and river suspended particulates

Core KZR-23 (5°40′S, 10°38′E; ~2220 m water depth; ~20 m long) was recovered during the ZAIROV cruise (2000; R/V *L'Atalante*), from a terrace lying at ~380 m above the thalweg, i.e. the deepest part of the Congo submarine canyon (Fig. 2). KZR-23 is mostly composed of homogeneous organic-rich fine-grained sediment, with minor contributions from diatoms and radiolaria. Most likely, the high total organic carbon content (2.7 ± 0.2 wt%) resulted in active early diagenetic processes within the sediment, even after core recovery and subsequent storage, which probably led to poor preservation of the rare foraminifera and other biogenic carbonate materials that were initially present. As a consequence, it is characterized by very low bulk sediment CaO contents (mean 0.5 ± 0.2 wt%). A major turbidite sequence was identified at about 17 mbsf (Babonneau et al., 2004), so that only the upper ~16 m of the core were investigated during the course of this study in order to avoid analysis of any disturbed sediment horizons.

A series of suspended river particulate samples from the Congo River watershed were also analyzed during this study. These samples were collected during the TransCongo expeditions (PI: A.V. Borges; Fig. 1B). TransCongo I (December 2013) consisted in a 1700-km transect across the river basin from Kisangani to Kinshasa, while TransCongo III (June 2015) was conducted in the Kasai River watershed. A total of 17 suspended particulates were collected using 15-L polyethylene reservoirs along the main course of the Congo and the Kasai rivers, and at the end point of their largest tributaries (Fig. 1B; Table 1). One sample was collected from the main stem of the Congo River at Kisangani (#3; sample number refers to Fig. 1B and Table 1) and is assumed to be representative of the sediment exported from the upstream Upper Congo

Table 1
Geochemical composition of river suspended sediments from the Congo Basin.

# River	Area (10^3 km^2)	Lat (°N)	Long (°E)	Bulk Al/K	^{143}Nd/^{144}Nd clay	2 SE (10^{-6})	ε_{Nd}	La	Ce	Pr	Nd	Sm	Eu	Gd	Tb	Dy	Ho	Er	Yb	Lu	$(Nd/Yb)_N$[a]
TransCongo river particulates																					
1 Tshopo	19	0.56	25.12	5.7	0.511968	7	−12.9	43.82	73.69	10.14	35.38	6.51	1.38	5.33	0.80	4.63	0.87	2.49	2.52	0.37	1.30
2 Lindi	39	0.57	25.12	7.2	0.511642	11	−19.3	30.78	46.59	5.72	18.67	3.22	0.77	2.66	0.40	2.23	0.43	1.20	1.21	0.17	1.42
3 Lualaba	1035	0.58	24.76	6.8	0.512044	10	−11.4	36.04	79.33	7.01	23.16	4.14	0.96	3.28	0.51	2.88	0.55	1.55	1.64	0.23	1.30
4 Lomami	116	0.77	24.27	9.6	0.512034	8	−11.6	29.79	48.87	6.02	19.67	3.48	0.79	2.93	0.45	2.62	0.57	1.71	1.88	0.27	0.96
5 Aruwimi	122	1.23	23.62	14.1	0.511466	12	−22.7	26.08	49.90	4.86	16.07	2.79	0.64	2.21	0.33	1.85	0.37	1.07	1.18	0.17	1.26
6 Itimbiri	57	2.06	22.70	14.6	0.511542	5	−21.2	59.02	82.65	10.20	32.41	5.23	1.07	3.89	0.57	3.15	0.61	1.74	1.78	0.25	1.68
7 Mongala	53	1.91	19.82	7.3	0.511987	22	−12.5	–	–	–	–	–	–	–	–	–	–	–	–	–	–
8 Lulonda	86	0.68	18.40	11.6	0.511775	6	−16.7	–	–	–	–	–	–	–	–	–	–	–	–	–	–
9 Ruki	179	0.07	18.32	13.8	0.511847	9	−15.3	–	–	–	–	–	–	–	–	–	–	–	–	–	–
10 Oubangui	640	−0.49	17.70	12.8	0.511744	9	−17.3	27.01	39.72	4.89	16.43	2.89	0.63	2.45	0.38	2.33	0.48	1.41	1.54	0.23	0.98
11 Kasai	890	−3.18	16.20	11.2	0.511875	6	−14.7	37.46	61.48	7.47	25.92	4.17	0.94	3.42	0.43	2.57	0.51	1.49	1.54	0.23	1.54
12 Kwango	176	−3.41	17.33	–	0.511942	9	−13.4	–	–	–	–	–	–	–	–	–	–	–	–	–	–
13 Kwilu	96	−3.39	17.41	–	0.511910	12	−14.0	–	–	–	–	–	–	–	–	–	–	–	–	–	–
14 Loange	42	−4.30	20.03	–	0.512130	15	−9.8	–	–	–	–	–	–	–	–	–	–	–	–	–	–
15 Upper Kasai	245	−4.36	20.58	–	0.511771	17	−16.8	–	–	–	–	–	–	–	–	–	–	–	–	–	–
16 Sankuru	148	−4.28	20.44	–	0.511701	13	−18.1	–	–	–	–	–	–	–	–	–	–	–	–	–	–
17 Kasai	890	−3.17	16.21	–	0.511822	25	−15.8	–	–	–	–	–	–	–	–	–	–	–	–	–	–
Lake Kivu sediment		−1.90	29.00	n.d.	0.512234	7	−7.7	26.40	53.26	5.33	18.64	3.24	0.76	2.68	0.34	1.79	0.33	0.93	0.93	0.14	1.84

[a] Normalized to World River Average Silt (WRAS; Bayon et al., 2015).

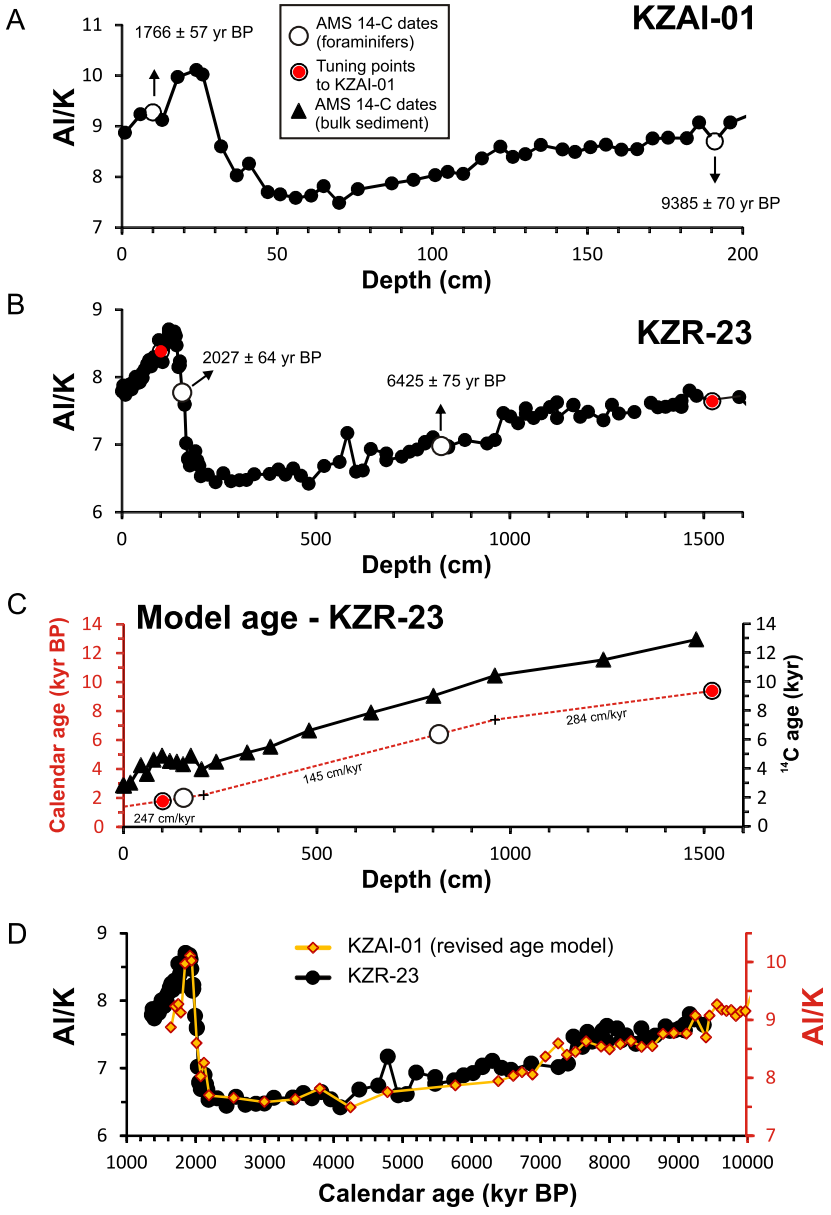

Fig. 3. Age model for core KZR-23. (A) Core KZAI-01 Al/K profile (Bayon et al., 2012) and age control points used for KZR-23 age model. (B) Core KZR-23 Al/K profile (this study), AMS^{14}C dates on mixed foraminifer fractions, and age control points derived from core KZAI-01. (C) Age vs depth relationship for 1) Mixed foraminifera fractions and age control points (in red), and 2) bulk C_{org} samples. (D) Calibrated age profile for Al/K in core KZR-23 and core KZAI-01 (revised). (For interpretation of the colors in the figure(s), the reader is referred to the web version of this article.)

(Lualaba) watershed. After settling, suspended particles were transferred into smaller polyethylene bottles, prior to being centrifuged at the laboratory within 50 ml centrifuge tubes and oven dried. In addition to these suspended particulate samples, one surface sediment from Lake Kivu (within the catchment area of the Lualaba River) collected in 2013 was also analyzed.

2.3. Age model

The chronology for core KZR-23 relies on two ^{14}C-AMS radiocarbon dates for mixed planktonic foraminifera fractions (150–160 depth and 800–820 depth), and tuning of the Al/K signal to that of core KZAI-01 (Fig. 3), also recovered off the Congo River mouth (Fig. 1B). One additional ^{14}C age was determined on echinoderm test fragments from the 800–820 depth interval, which confirmed the corresponding ^{14}C age on mixed foraminifera. These radiocarbon dates were converted into calendar ages with the Calib 7.1 program (Stuiver et al., 2017), applying the MARINE13 radiocarbon age calibration curve (Table S1). Additional constraints on sedimentation rates, obtained from ^{14}C-AMS ages of 21 bulk samples, were also used for establishing the age model (Fig. 3). Constant sedimentation rates were assumed between the 203–961 cm and 961–1481 cm depth intervals, on the basis that both sediment intervals exhibited linear 'depth' versus 'bulk $^{14}C_{org}$' relationships. While there is inherent uncertainty associated with the age model of KZR-23, due to its particular depositional setting dominated by terrigenous inputs and the poor carbonate preservation within the sediment, the timing of the high-Al/K episode in the upper part of the core (which is the main focus of the discussion below) is well constrained by the combination of two ^{14}C dates from KZR-23 and KZAI-01 (Fig. 3B). Note also that our age model indicates that the last ~1300 yrs are missing from the sediment record at site KZR-23 (Fig. 3D); a feature that we tentatively attribute to a decrease of sediment dynamics in the Congo submarine canyon over the recent period.

2.4. Major element inorganic analyses

A total of 140 bulk sediment samples from core KZR-23 were analyzed for major element concentrations at Ifremer, using wavelength-dispersive X-ray fluorescence (WD-XRF). The precision of measured Al/K ratios was assessed from replicate analyses of various KZR-23 samples during the course of 5 different analytical sessions (<5%; $N = 15$). The geochemical composition of bulk suspended sediments collected during the TransCongo I expedition was determined by inductively coupled plasma–atomic emission spectroscopy (ICP–AES) at the Royal Museum for Central Africa, with average accuracies typically below 5%. The results for Al/K ratios in TransCongo suspended particulates and core KZR-23 samples are listed in Table 1 and Table S2, respectively.

2.5. Rare earth elements and Nd isotopic measurements

All bulk sediment and river suspended particulate samples were treated using a sequential leaching procedure to remove biogenic, Fe–Mn oxyhydroxide and organic components (Bayon et al., 2002). Clay-size fractions were separated from the residual detrital material using low-speed centrifugation (Bayon et al., 2015). Between 40–80 mg of the obtained clay-size fractions were digested by alkaline fusion for rare earth elements (REE) and Nd isotopic measurements. Note that due to small sample weight (<15 mg), two suspended particulate samples collected from rivers draining the central depression of the Congo Basin (Lulonda and Ruki) were digested using concentrated HF:HCl solution without any initial leaching or grain-size separation.

Rare earth element concentrations were determined on a Thermo Scientific Quad X-Series 2 at the Royal Museum for Central Africa. The REE abundances were determined with a precision better than 5% and normalized to World River Average Silt (WRAS; Bayon et al., 2015). Neodymium was isolated using conventional ion chromatography and isotopic measurements were performed at the Pôle Spectrométrie Océan (Brest), using a Thermo Scientific Neptune multi-collector ICPMS. Nd isotopic compositions were determined using sample-standard bracketing, by analyzing JNdi-1 standard solutions every two samples. Mass-bias corrected values for $^{143}Nd/^{144}Nd$ were normalized to a JNdi-1 value of $^{143}Nd/^{144}Nd = 0.512115$ (Tanaka et al., 2000). Analyses of an in house (SPEX-Nd) standard solution during the course of this study (2 analytical sessions) gave $^{143}Nd/^{144}Nd$ of 0.511709 ± 0.000007 (2 SD, $n = 16$), corresponding to an external reproducibility of $\sim \pm 0.15\varepsilon$ (2 SD). Epsilon Nd values (ε_{Nd}) were calculated using $^{143}Nd/^{144}Nd = 0.512630$ (Bouvier et al., 2008). Neodymium isotopic data are reported in Table 1 (TransCongo suspended particles) and Table S2 (KZR-23 samples). Together with results published earlier on another series of suspended particulate samples from the Congo River (Allègre et al., 1996), these datasets were used to calculate end-member Nd isotopic compositions for the three main tributaries of the Congo River (Lualaba, Oubangui and Kasai; see Table S3).

2.6. Calculation of apparent initial radiocarbon ages

The apparent initial ages of the terrestrial organic matter exported by the Congo River were calculated using bulk AMS radiocarbon data and corresponding depositional ages in KZR-23 inferred from our model age (Table S4). These apparent ages correspond to the age of a sedimentary organic fraction at the time of deposition. An apparent initial age of several thousand years (as will be reported below for core KZR-23) generally indicates that rivers were transporting pre-aged plant organic matter from soils at the time of sediment deposition (Schefuß et al., 2016; Winterfeld et al., 2018). Following the approach described in these latter studies, the apparent initial ages (yr) were calculated after correction of the atmospheric radiocarbon content at the time of sediment deposition ($\Delta^{14}C_{atm}$), derived from the Intcal13 southern hemisphere atmospheric data (Table S4):

$$^{14}C\ age_{apparent}\ (yr) = -8{,}033 \times \ln\left[\left(1 + \Delta^{14}C_{initial}/1000\right)/\left(1 + \Delta^{14}C_{atm}/1000\right)\right]$$

where $\Delta^{14}C_{initial}$ corresponds to the initial radiocarbon content of bulk KZR-23 samples calculated using the following equation (Stuiver and Pollach, 1977):

$$\Delta^{14}C_{initial}\ (‰) = 1000 \times \left(Fm/e^{((2015-1950)/8267)} - 1\right)$$

2.7. n-alkane isotope analyses and BIT-index

Bulk organic carbon contents (%OC) in core KZR-23 were determined at KU Leuven using a Thermo Flash HT/EA equipped with a Costech zero-blank analyzer (Table S4). For *n*-alkane isotope analyses, lipids were extracted using a Dionex accelerated solvent extractor with 9:1 (v/v) dichloromethane (DCM)/methanol (MeOH). Asphaltenes were precipitated from the total lipid extract and hexane-soluble fractions were subsequently saponified with 6% KOH in MeOH for 2 h at 85 °C. Saturated hydrocarbon and polar lipid fractions were obtained from neutral lipids using silica column chromatography by elution with hexane and DCM/MeOH (1:1), respectively. Saturated hydrocarbon fractions were subsequently eluted on $AgNO_3$-coated silica. Quantification of long-chain *n*-alkanes was achieved using a ThermoFisher Scientific Focus gas chromatograph equipped with an Rxi-5 ms 30× column (30 m, 0.25 mm, 0.25 µm) and a flame ionization detector. Identification and quantification of compounds was done by comparison to retention times and peak areas of an external *n*-alkane standard mixture. Maximum quantification uncertainty is 5%. The *n*-C_{29} alkane was consistently the most abundant plant-wax compound in all samples and isotope analyses were therefore focused on this compound. Hydrogen isotope analyses (δD) were conducted at least in duplicate on a ThermoFisher Scientific MAT 253 isotope ratio mass spectrometer (IRMS) coupled via a GC Isolink operated at 1420 °C to a ThermoFisher Scientific Trace GC at MARUM, Bremen. δD compositions were measured against calibrated H_2 reference gas and δD values are reported in per mill (‰) versus Vienna Standard of Mean Ocean Water (VSMOW; Table S5). Average standard deviation for replicate δD measurements is 1‰ for the *n*-C_{29} alkane. The internal standard (squalane) yielded an accuracy of +2‰ and a precision of 3‰ ($n = 94$). An external standard mixture with known δD values was analyzed repeatedly every six runs, yielding a long-term mean standard deviation of <3‰ and a mean deviation of <1‰ from reference values.

Compound-specific stable carbon isotope analyses were carried out at least in duplicate on a ThermoFisher Scientific MAT 252 isotope ratio mass spectrometer coupled via a GC-C combustion interface with a nickel catalyzer operated at 1000 °C to a ThermoFisher Scientific Trace GC at MARUM, Bremen. $\delta^{13}C$ values were calibrated against CO_2 reference gas of known isotopic composition and $\delta^{13}C$ values are reported in per mill (‰) against Vienna PeeDee Belemnite (VPDB; Table S5). Average standard deviation of $\delta^{13}C$ values for the *n*-C_{29} alkane is 0.1‰. The internal standard (squalane) yielded an accuracy of +0.4‰ and a precision of 0.4‰ ($n = 94$). An external standard mixture was analyzed repeatedly every 6 runs and yielded a long-term mean standard deviation of 0.2‰ with a mean deviation of 0.1‰ from the reference values.

Branched and isoprenoid glycerol dialkyl glycerol tetraether lipids (GDGTs) were analyzed in the polar fractions filtered through

4 µm pore size PTFE filters. GDGTs were analyzed by high-performance liquid chromatography (HPLC) mass spectrometry (MS) using a method slightly modified from Hopmans et al. (2004). GDGTs analyses were conducted using an Agilent 1200 series HPLC system coupled with an Agilent 6120 mass selective detector (MSD) system. The branched and isoprenoid tetraether (BIT) index was calculated according to Hopmans et al. (2004). Corresponding BIT-index values are reported in Table S5.

2.8. Pollen

Palynological sample preparation followed standard procedures, whereby samples of 0.3–4.2 g dry sediment were decalcified with diluted HCl and subsequently treated with concentrated HF to remove silicates. Samples were sieved using ultrasonic sieving over a screen removing particles smaller than 10–15 µm. Pollen samples were mounted in glycerol and microscopically examined at 400× and 1000× magnification. Pollen percentages were calculated based on the total number of pollen and spores. Confidence intervals (95%) were calculated after Maher (1972). Pollen grains were identified using several publications (see supplementary information), the African Pollen Database, and the reference collection of the Department of Palynology and Climate Dynamics of the University of Göttingen. A list of 114 arboreal pollen taxa (Vincens et al., 2007) and a list of 22 pollen taxa from the pioneer forest (Dalibard et al., 2014) are given in Table S6. The percentage means for selected pollen taxa and groups used in this study are listed in Table S7.

3. Results and proxy interpretation

3.1. Past weathering and erosion changes: Al/K, BIT-index and initial bulk organic matter apparent ^{14}C ages

Bulk sediment aluminium-to-potassium ratios (Al/K) in sediments and river suspended matter can provide constraints on chemical weathering intensity. Potassium is highly mobile during chemical weathering and typically depleted in soils, while aluminium is one of the most immobile elements and is incorporated into secondary clay minerals (Govin et al., 2012). Direct comparison of Al/K values measured in river suspended particulates and marine sediments may be complicated by various lithological and grain-size effects (Bouchez et al., 2011). However, the evolution of Al/K ratios and other weathering proxies in sedimentary records is generally considered to reflect past fluctuations in alteration processes coupled with changing hydroclimate and vegetation patterns on continents (e.g. Schneider et al., 1997; Bayon et al., 2012; Ivory et al., 2017). At the Congo margin, the utility of Al/K for reconstructing past chemical weathering has been demonstrated using Hf isotopes, which represent another powerful indicator for silicate weathering intensity (Bayon et al., 2009, 2012). In core KZR-23, bulk sediment Al/K ratios progressively decrease between ~10.0 and 2.2 thousand years ago (from 7.6 to 6.4; Fig. 4A), suggesting decreasing soil weathering in response to a general drying trend. The most striking feature of the Al/K profile is the sudden and pronounced increase between 2.2 and 1.8 kyr BP (up to Al/K ~8.7), which indicates export of highly weathered sediments at that time. Unequivocally, this episode corresponds to the so-called third millennium BP weathering event identified previously in Congo fan sediments (Bayon et al., 2012). The timing of the Al/K peak slightly differs between the two sediment records: about 2.3 kyr BP for core KZAI-01 (Bayon et al., 2012) and 1.9 kyr BP for KZR-23. This difference arises from minor age model offsets, but the revised age model reported here is better constrained by AMS radiocarbon data and hence represents a more accurate temporal estimate for the event (Fig. 2).

Sedimentation at site KZR-23 is also characterized by substantial inputs of terrestrial organic matter (OM), as inferred from the branched and isoprenoid tetraether (BIT) index. In marine sediment records, the BIT index represents a measure of the relative proportion of soil-derived (BIT ~0.8–1) versus marine (BIT ~0–0.2) organic matter (Hopmans et al., 2004). In core KZR-23, the BIT index remains high (0.76 ± 0.05; 1 SD) throughout the entire Holocene (Fig. 4B), indicating that accumulation of bulk OM at this site was dominated by terrestrial inputs. In this context, the development of the age of organic matter deposited at the studied site (as inferred from the difference between bulk sedimentary OM radiocarbon ages and corresponding depositional ages; see section 2.6), can provide useful information on past erosion processes of pre-aged terrestrial OM in the Congo Basin (Fig. 4C). Core KZR-23 sediments display apparent initial bulk OM ages ranging from ~1400 to 3000 ^{14}C yr (Table S4), which suggest that the Congo River has been exporting aged organic matter throughout the Holocene period in accordance with earlier findings (Schefuß et al., 2016). At site KZR-23, the age of soil-derived OM is about 2,900 ± 200 ^{14}C yr (1 SD) between 10.0 and 5.0 kyr BP, then progressively decreases (down to ~1600 ^{14}C yr) during the mid-to-late Holocene period, before increasing suddenly after 2.2 kyr BP (up to ~2,700 ^{14}C yr). This trend differs from that obtained from bulk OM and compound-specific radiocarbon analyses in the nearby core GeoB6518-1 (Schefuß et al., 2016). The cause of this discrepancy is unclear but likely relates to differences in sedimentation rates and associated diagenetic processes between the two sites. To some extent, the inherent uncertainty associated with our age model for KZR-23 could also account, at least partly, for the observed discrepancy between KZR-23 and GeoB6518-1 bulk OM radiocarbon records. Nevertheless, the sudden shift towards greater initial OM ages after 2.2 kyr BP, coinciding with evidence for export of highly weathered sediments (as inferred from Al/K ratios), strongly suggests that enhanced erosion of pre-aged terrigenous OM occurred in the Congo Basin at that time.

3.2. Vegetation patterns: Pollen and $\delta^{13}C_{wax}$

Information on past vegetation patterns in the Congo Basin can be inferred from both pollen assemblages and compound-specific stable carbon isotope ratios of plant lipids. The mid-Holocene period appears to display slightly higher relative abundances of tree pollen taxa, which mainly reflect increased proportions of dry forest woodlands relative to the rainforest trees (Fig. 4D; Table S7). However, pollen assemblages in KZR-23 do not reveal any clear long-term trend during most of the Holocene, with abundances of tree pollen, rainforest and forest/woodland taxa displaying relatively limited downcore variations (Fig. 4D). Similarly, stable carbon values ($\delta^{13}C$) of the n-C_{29} alkanes display near constant values in core KZR-23 (−34.1 ± 0.3‰ VPDB; Table S5). Although higher resolution profiles for pollen and/or n-alkanes $\delta^{13}C$ would be required to more accurately reconstruct past vegetation patterns in the Congo Basin, these results suggest that limited vegetation changes occurred in the central African rainforest during the Holocene. However, like the weathering and erosion proxy data reported above, pollen-based vegetation patterns also demonstrate a significant shift after 2.2 kyr BP, characterized by a reduction of tree pollen (Fig. 4D), an increase of oil palm (from near-zero values to >1%; Fig. 4E) and forest pioneer species (from ~2 up to 6%; Fig. 4E), followed after 2 kyr BP by a pronounced expansion of grasses (from ~6 up to 16%; Fig. 4D). In tropical Africa, oil palm and other pioneer species can usually rapidly colonize areas that have been subject to forest degradation (Sowunmi, 1999; Maley, 2001). Therefore, their presence in core KZR-23 after 2.2 kyr BP provides evidence for forest decline in the Congo Basin during the late Holocene.

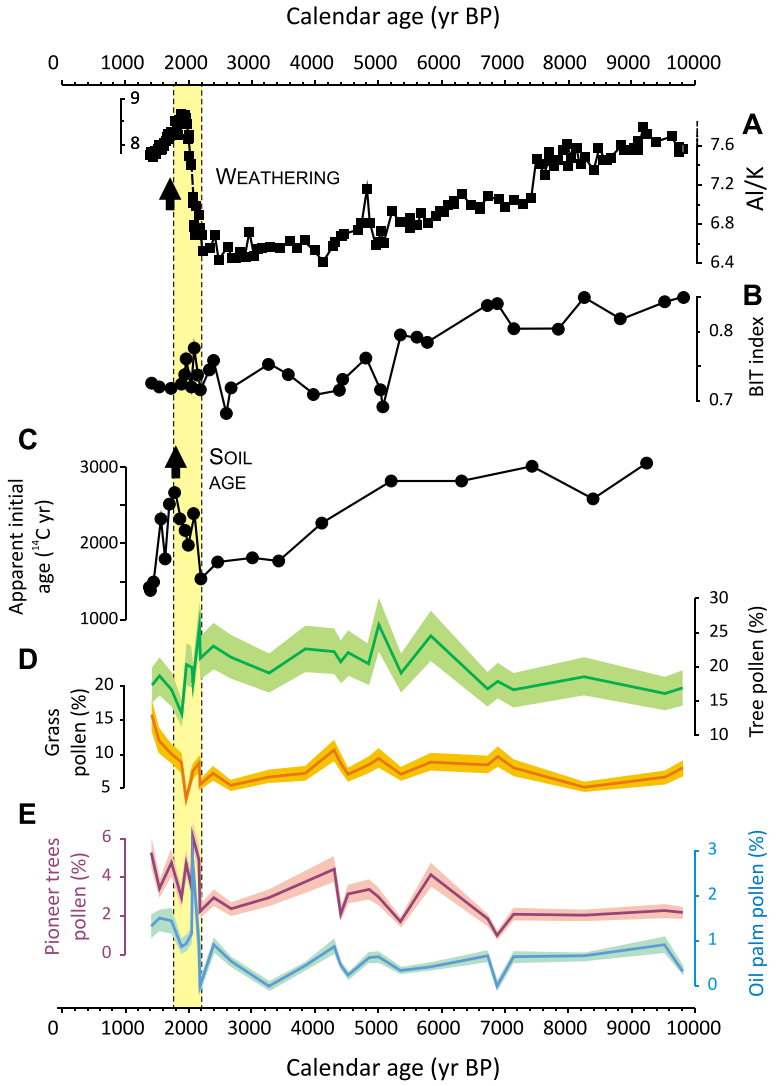

Fig. 4. Core KZR-23 proxy records for the evolution of past erosion and vegetation patterns in Central Africa. (A) Bulk sediment Al/K ratios indicate past changes in chemical weathering and degree of alteration of soils. Note that two different Y-axis scales used for the late Holocene (from 7.5 to 9), and the rest of core KZR-23. (B) BIT index values calculated from GDGTs data, representing the relative proportion of terrestrial (BIT ~0.8–1) versus marine (BIT ~0–0.2) OM in bulk sediment. (C) Apparent initial ages of bulk sediment organic carbon. (D) Percentages of pollen taxa for trees, including rainforest and woodlands, normalized to total pollen counts. Shading indicates 95% confidence intervals. Percentages of pollen taxa for Poaceae (grasses). (E) Percentages of pollen taxa from pioneer forest and oil palm (*Elaeis guineensis*). The vertical yellow band corresponds to the Late Holocene 'weathering' event inferred from Al/K ratios.

3.3. Sediment provenance proxies: Nd isotopes and rare earth elements

The suite of river particulate samples collected within the Congo watershed was used to identify the characteristic Nd isotope and REE signatures of each major sub-basin (Table 1). Measured Nd isotopic compositions range from ε_{Nd} −22.7 (Aruwimi; #3) to −9.8 (Loange; #14), in agreement with previously published results for other river suspended particles from the Congo Basin (Allègre et al., 1996) and a recent regional synthesis for Nd isotopes in Central Africa (Thiéblemont et al., 2014). Our data indicate that the Oubangui, Kasai and Upper Congo (Lualaba) rivers, which represent the most important tributaries of the Congo in terms of solid particulate discharge (Laraque et al., 2009), are characterized by distinctive Nd isotopic signatures ($\varepsilon_{Nd} = -17.6 \pm 0.4$; -15.5 ± 0.7 and -11.4 ± 0.2, respectively; see Table S3 for the definition of the end-members). While also representing a large part of the Congo watershed, the rivers draining the Cuvette Centrale (e.g. Ruki, Lulonda, Mongala) carry very little total suspended material in comparison (Laraque et al., 2009), and hence contribute negligibly to the total solid discharge of the Congo River. The Oubangui, Kasai and Lualaba river particles also display differences in WRAS-normalized REE patterns, with Oubangui suspended particles being characterized by slightly depleted mid REE (MREE) normalized-abundances relative to light and heavy REE, and particulate matter from the Kasai and Lualaba rivers exhibiting more pronounced LREE enrichment relative to the other REE (Fig. 5). This results in suspended particulates from the Oubangui, Kasai and Lualaba being characterized by distinctive neodymium-to-ytterbium ratios (taken here as a measure of the relative enrichment of LREE over HREE), with $(Nd/Yb)_N$ of ~0.98, 1.54, and 1.30, respectively (Table 1). Overall, these characteristics indicate that both Nd isotopes and REE can be used to reconstruct past changes between northern (Oubangui) and southern/eastern (Lualaba and Kasai) sedimentary inputs to site KZR-23, and thus to provide information on the geographic origin of the sediments exported by the Congo River.

In core KZR-23, Nd isotopes display overall homogeneity with an average ε_{Nd} value of -15.6 ± 0.1 (1SD; Fig. 6A), which suggests that sediment provenance, and hence the mean latitudinal position of the rainbelt over the Congo Basin, have remained mostly

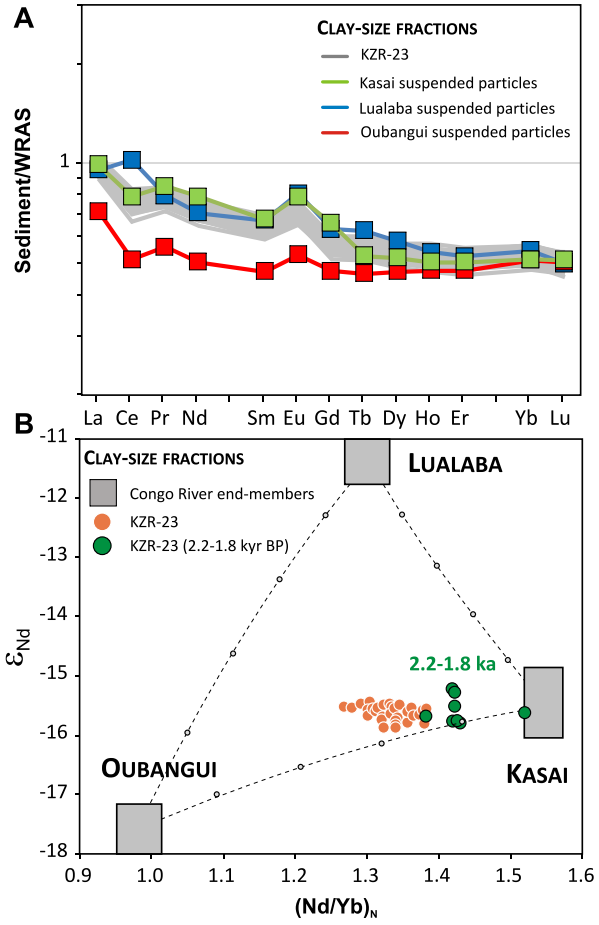

Fig. 5. Rare earth element constraints on sediment provenance changes. (A) Rare earth element abundances of clay-size fractions from river suspended material in the Congo Basin (squares) and core KZR-23 sediments (gray lines), normalized to World River Average Silt (Bayon et al., 2015). (B) Plot of ε_{Nd} versus $(Nd/Yb)_N$ ratios for KZR-23 detrital fractions. The three main sources of terrigenous material to the solid load exported from the Congo River Basin (Oubangui, Kasai and Lualaba) are plotted for comparison. Mixing lines between the three end-members are shown, with small gray circles corresponding to 20%, 40%, 60% and 80% relative contributions.

unchanged over the last 10 thousand years. Minor ε_{Nd} fluctuations occur downcore, in particular around 2 kyr BP, when a subtle but significant shift towards more radiogenic signatures (from −15.8 to −15.2) indicates a period of enhanced relative sediment contributions from the southern and/or eastern parts of the Congo watershed. This assumption is further supported by the $(Nd/Yb)_N$ profile in KZR-23, which similarly displays a sudden increase at about 2.2 kyr BP (Fig. 6B), indicative of enhanced relative sediment input from the Kasai sub-basin. Quantitative constraints on past provenance changes in core KZR-23 can be obtained using a mixing model that combines ε_{Nd} and $(Nd/Yb)_N$ end-member compositions for the Oubangui, Lualaba and Kasai rivers (Fig. 5B). These results suggest that sedimentation at site KZR-23 has been dominated by inputs from the Kasai River during the entire Holocene, with an average contribution of about 68 ± 10%, while Oubangui and Lualaba rivers accounted for the remaining ∼23 ± 8% and 9 ± 4%, respectively (Fig. 7A). Relative sedimentary inputs from the Oubangui and Kasai rivers display little long-term fluctuations between 10 and 2.2 kyr BP (Fig. 7A), in contrast with sediment discharge associated with the Lualaba River, which decreases significantly from the mid-Holocene to 2.2 kyr BP (from about 16% to 5%). As suspected from $(Nd/Yb)_N$ ratios, our mixing model also indicates an abrupt shift towards increasing sediment contributions from the Kasai region between ∼2.2 to 2.0 kyr BP, immediately followed by a sharp decrease (down to ∼50%) and enhanced export of particles from the Lualaba and Oubangui catchment areas (Fig. 5B; Fig. 7A).

3.4. Hydroclimate δD_{wax} record

Information on past hydrological changes can be inferred from the application of hydrogen isotope analysis of plant wax derived biomarkers (δD_{wax}, in ‰ relative to VSMOW). In tropical areas, hydrogen isotope abundances in plant waxes are mainly controlled by rainfall amounts and the precipitation–evaporation balance, therefore reflecting predominantly continental hydrological changes (Sachse et al., 2012). As already reported in earlier studies (Schefuß et al., 2005), the long-term precipitation trend inferred from δD_{wax} in core KZR-23, from about −150‰ in the early Holocene to −134‰ in the more recent period (Fig. 6C), indicates progressively decreasing rainfall since about 6.5 kyr BP in response to declining northern hemisphere summer insolation. This general drying trend is punctuated by a ∼10‰ shift towards heavier δD_{wax} compositions between 7.5 and 6.5 kyr BP, which probably indicates slightly reduced precipitation levels at that time. Another shift towards slightly more depleted δD_{wax} values occurred between 2.2 and 1.4 kyr BP (i.e. the most recent sediment in core KZR-23), but its amplitude is small (less than 5‰), so that it could also reflect isotopic effects due to changes in basin-internal rainfall patterns. At present, precipitation in the Kasai watershed is isotopically depleted relative to rainfall in the Oubangui and Lualaba catchments (http://wateriso.utah.edu/waterisotopes/media/IsoMaps/jpegs/h_Africa/Hma_Africa.jpg). A decrease in rainfall in the latter sub-catchments could thus have led to a shift towards relatively depleted δD_{wax} signature recorded in KZR-23.

4. Discussion

4.1. Evidence for Late Holocene climate change in the Congo Basin

Taken together, Nd isotopes and REE data provide evidence for climate instability in the Congo Basin from about 2.2 kyr BP onwards, presumably associated with changing discharge patterns in different parts of the watershed. In agreement with δD_{wax}, Nd isotopes and REE suggest that the period after ∼2.2 kyr BP was associated with decreasing rainfall in the northern and eastern regions drained by the Oubangui and Lualaba, respectively, and relatively elevated discharge from the Kasai sub-basin. At the scale of the vast Congo Basin, this event does not appear to have been related to any substantial change in total basin-integrated precipitation levels, as inferred from the relatively small shift in δD compositions of plant leaf waxes. For this time interval, there is plenty of evidence for contrasting patterns of climate change across Central Africa. In western equatorial Africa, this period was accompanied by intense land surface processes associated with the formation of coarse-grained deposits, followed by rapid deposition of a cover horizon of potential aeolian origin, which were both interpreted as the consequence of abrupt climate deteriorations (Thiéblemont et al., 2013, 2014; Maley et al., 2018). Instead, in eastern tropical Africa, precipitation proxy records generally indicate wetter conditions during this period (e.g. Tierney et al., 2011; Foerster et al., 2012). In particular, our inferred late Holocene hydroclimatic shift in the Congo Basin coincides with a period of markedly increasing rainfall at the Chew Bahir Basin in southern Ethiopia (Foerster et al., 2012; Fig. 7B); an event that was attributed to strengthening of El Niño-Southern Oscillation (ENSO). The distribution of precipitation in tropical East Africa is indeed partly driven by tropical Indo-Pacific climate and affected by ENSO (Preethi et al., 2015). While eastern equatorial Africa tends to experience greater than normal precipitation during an ENSO event, south-eastern African regions display drier than normal conditions

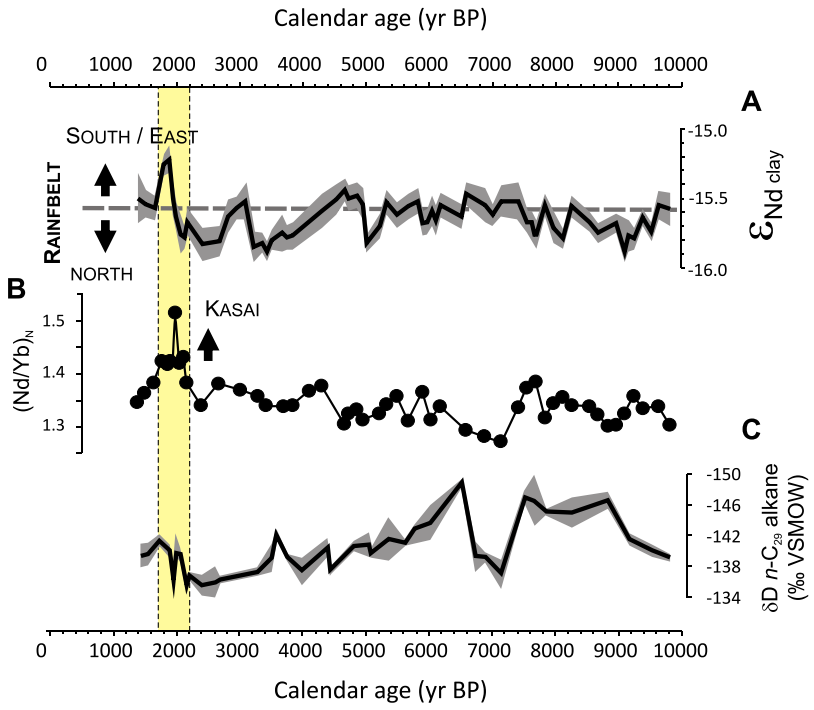

Fig. 6. Proxy records for sediment provenance and hydroclimate in KZR-23 during the Holocene. (A) Nd isotopes (ε_{Nd}) in fine-grained detrital fractions represent relative sediment inputs from the Ubangui (−17.6), Kasai (−15.5), and Lualaba (−11.4) source areas and provide information on past shifts of the rainbelt from northern to southern/eastern parts of the watershed, respectively. Analytical uncertainty if shown in gray shading. (B) Evolution $(Nd/Yb)_N$ in detrital fractions as proxy for sediment provenance. (C) Hydrogen stable isotope composition of leaf-wax *n*-C_{29} alkanes (δD_{wax}; in ‰ VSMOW), with gray shading corresponding to analytical uncertainty. More negative values indicate wetter conditions. The vertical yellow band corresponds to the Late Holocene 'weathering' event inferred from Al/K ratios.

(Ropelewski and Halpert, 1987; Nicholson and Kim, 1997). One of the presumed mechanisms behind these climate anomalies is that ENSO events are associated with an eastward migration of the Congo Air Boundary (CAB), i.e. the convergence zone that marks the confluence of Indian Ocean air with air masses derived from the Congo Basin (Ropelewski and Halpert, 1987; Tierney et al., 2011). To date, the impact of ENSO events on central African climate remains largely unknown, due to a lack of continuous long-term meteorological data for the Congo Basin. However, such a link has been already evoked (Mbuebue et al., 2016), which could possibly account for substantial rainfall changes in Central Africa, drawing moisture away from the central and eastern parts of the Congo basin towards eastern equatorial Africa (Tierney et al., 2011; Junginger et al., 2014). While the mid-Holocene period was globally characterized by weak El Niño activity, palaeoclimate records from key ENSO-sensitive regions generally indicate much stronger and/or more frequent El Niño events between 2000 and 1000 yrs ago (Lu et al., 2018; see Fig. 7C–E and references therein). A late Holocene strengthening of ENSO would thus be coherent with our finding, based on Nd isotopes and REE, that precipitation levels abruptly decreased in both the Lualaba and Oubangui watersheds from ∼2200 yr BP leading to a relative increase of the signal from the Kasai sub-basin. To summarize, we tentatively propose here that increasing El Niño activity during the late Holocene possibly played an important role in driving the sudden reorganization of rainfall patterns across the Congo watershed after ∼2.2 kyr BP, as inferred from our hydroclimate proxy records in core KZR-23.

4.2. A climatic forcing for the eastward Bantu migration across Central Africa?

Collectively, our proxy records for past vegetation, erosion and weathering patterns in Central Africa clearly show that major environmental disturbances occurred between about 2.2 and 1.6 kyr BP, hence contemporaneously with the period of presumed climate instability inferred from our Nd isotope and REE data. The timing of this environmental crisis is slightly younger, but consistent with previous evidence from a number of terrestrial sites across Central Africa, which all point to important forest retreat and erosive surface processes between about 2.6 and 2.0 kyr BP (Vincens et al., 1998; Maley, 2002, 2018; Thiéblemont et al., 2013; Bostoen et al., 2015). Importantly, this period also coincides remarkably well with the first major immigration wave of Iron Age communities into the rainforest, as inferred from recent syntheses of radiocarbon dates for archaeological sites in western Central Africa (Fig. 7F; Oslisly et al., 2013; Morin-Rivat et al., 2014; Garcin et al., 2018). Evidence for simultaneous occurrence of changes in hydroclimate, vegetation and erosion within the Congo Basin during this time interval thus suggests a close connection with the Bantu migrations across the central African rainforest. We speculate that changing hydroclimate patterns in the Congo's inland basin during the third millennium BP may have played an important role in driving the Bantu migration across Central Africa. The evolution of sediment provenance changes reconstructed from Nd isotopes and REE at site KZR-23 suggests that precipitation levels in the northern and eastern regions of the Congo basin became severely reduced from ∼2.2 and 2.0 kyr BP, while comparatively wetter conditions prevailed in the Kasai catchment area (Fig. 7A). As proposed earlier (Bostoen et al., 2015), such a climatic reorganization, which we tentatively attribute to enhanced ENSO variability, could have led to forest retreat in these regions, possibly triggering large-scale displacement of Bantu-speaking populations at that time through opening of savanna corridors. Albeit speculative, this hypothesis would be coherent with phylogenetic investigations of their dispersal route, which suggest that after following a southeastward direction first, the Bantu farmers then moved eastwards to reach the eastern fringe of the Congo Basin by about 2000 yr ago (Grollemund et al., 2015).

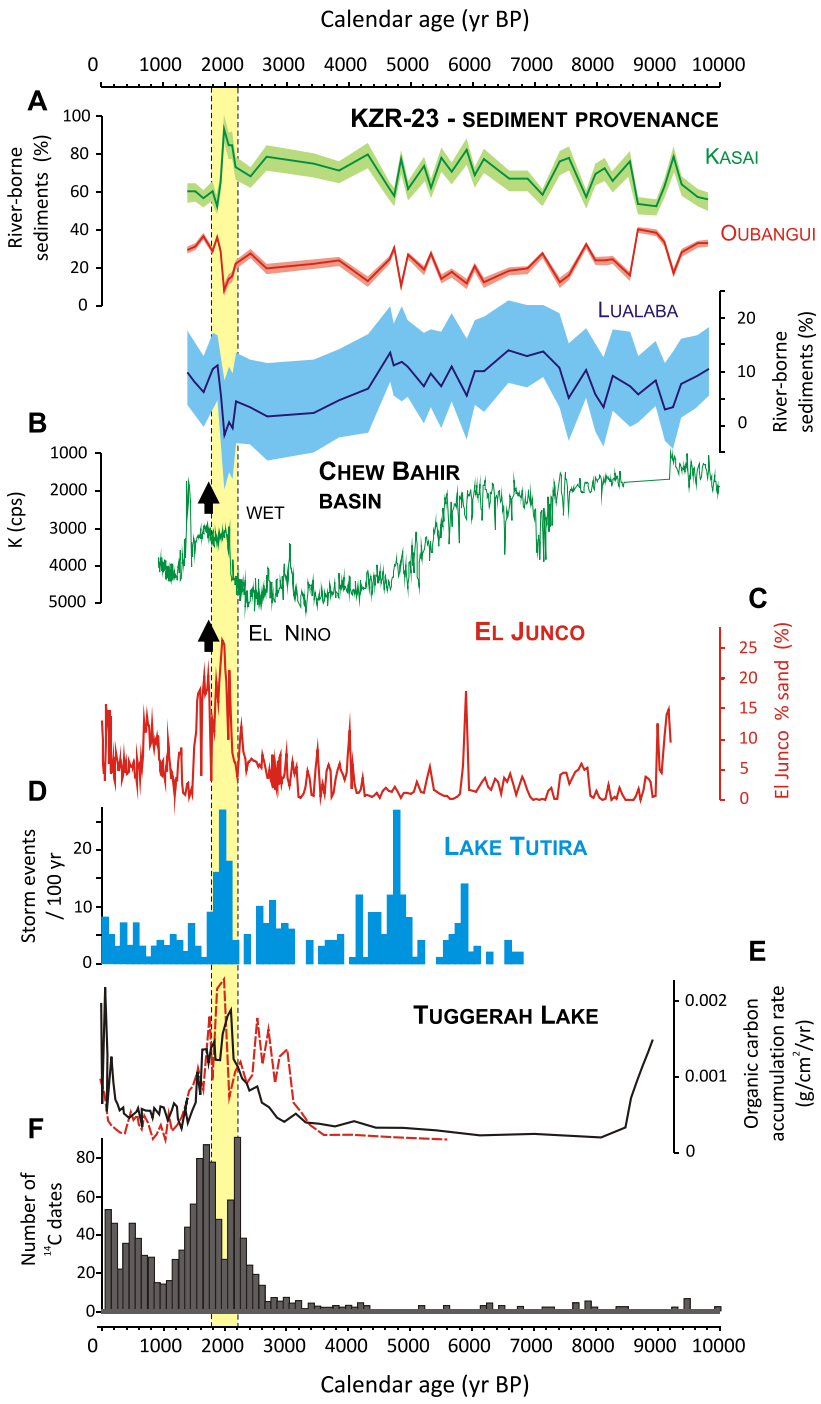

Fig. 7. Reconstructed past sediment provenance changes in KZR-23, compared to other Holocene records for palaeoclimate and iron age human settlements in Central Africa. (A) Relative percentage contributions of sediment from the Kasai, Oubangui and Lualaba catchment areas calculated using a mixing model combining ε_{Nd} and $(Nd/Yb)_N$ end-member compositions. Note the different scale for the Lualaba % sediment contribution. Shading indicates the uncertainty on modeled values when taking into account uncertainties (1SD) on the Nd isotopic composition of sediment end-members. (B) Chew Bahir Basin potassium (K) record (note reverse scale) of past aridity in southern Ethiopia (Foerster et al., 2012). (C–E) Paleo-ENSO sediment records from Galapagos Lake El Junco (percent sand fraction; Conroy et al., 2008); Lake Tutira, New-Zealand (storm events per century; Gomez et al., 2012); Tuggerah Lake, Australia (ENSO associated changes in organic carbon accumulation rates; Macreadie et al., 2015). (F) Number of radiocarbon dates for archaeological sites in western Central Africa (Garcin et al., 2018). The vertical yellow band corresponds to the Late Holocene 'weathering' event inferred from Al/K ratios.

4.3. Climate versus human impacts on the late Holocene environments in Central Africa

Our multi-proxy investigation allows us to re-evaluate the hypothesis that humans may have been involved in the late Holocene crisis of the central African rainforest (Bayon et al., 2012; Garcin et al., 2018). The third millennium BP episode of forest clearance in Central Africa is generally attributed to enhanced aridity and/or more pronounced climate seasonality (e.g. Neumann et al., 2012; Bostoen et al., 2015; Maley et al., 2018). Similarly, increased storm activity related to enhanced rainfall seasonality has also been proposed as an explanation for the intense erosional events that took place during the late Holocene, which are now preserved as very coarse-grained sedimentary deposits in many upper soil sequences

across Central Africa (Thiéblemont et al., 2013; Maley et al., 2018). As suggested above, the late Holocene environmental changes in the Congo Basin, reconstructed from our proxy data, could also be explained by a prolonged phase of climate instability related to strengthening of ENSO. To a large extent, the observed changes in core KZR-23 after 2.2 kyr BP, including changes in vegetation patterns, could have been driven by an internal basin-wide shift of precipitation. In this context, the erosional material inferred from bulk OM radiocarbon and Al/K data after 2.2 kyr BP could correspond to remobilized pre-aged soils previously deposited in the Cuvette Centrale. This important storage reservoir for particulate OM has been forming since the early Holocene and is thought to be particularly sensitive to precipitation changes within the watershed (Schefuß et al., 2016; Hemingway et al., 2017; Dargie et al., 2017). In core KZR-23, the increase in bulk OM initial ^{14}C ages at 2.2 kyr BP coincided with markedly reduced sediment inputs from the Lualaba and the Oubangui watersheds (Fig. 7A), hence at a time when drier conditions probably prevailed in northern and eastern Central Africa. This particular climatic context could have resulted in a substantial drop of the water level within the Cuvette, which would have led to remobilization of pre-aged particulate OM and possibly highly weathered sediments.

While our results appear to provide support for the role of climate in the late Holocene rainforest crisis, the magnitude of the observed environmental signals, especially for Al/K ratios, still remains enigmatic and could point towards human imprint on the rainforest as suggested by Bayon et al. (2012) and more recently by Garcin et al. (2018). Compared to the Congo Basin, Lake Barombi has a much smaller catchment area and the development of human activities in this part of southwestern Cameroon during the third millennium BP most likely led to an amplified anthropogenic signal now recorded in the lake sediment deposits (Garcin et al., 2018). In contrast, the vastness of the Congo Basin and the diversity of vegetation patterns across its watershed probably acted as a buffer that dampened the anthropogenic signal exported by river sediments and pollen at that time. Nevertheless, settlements of Iron Age communities in the rainforest were accompanied by slash-and-burn practices and iron ore smelting, which locally led to woodland clearance (Oslisly et al., 2013; Lupo et al., 2015). Bayon et al. (2012) showed that the pulse of highly weathered material exported from the Congo Basin during the late Holocene had been unprecedented for at least the last 40 ka, and this was taken as evidence for large-scale human impact on central African landscapes. As proposed earlier (Sowunmi, 1999), the increasing abundance of oil palm pollen recorded at site KZR-23 after 2.2 kyr BP (Fig. 4E) could indicate local plant cultivation, although its expansion in the Congo Basin could also relate to climate deterioration and associated forest disturbance (Maley, 2001). While the forest decline during the late Holocene probably opened dispersal routes towards the east (Grollemund et al., 2015), the combination of presumed intensifying land-use and strengthening of ENSO variability, presumably associated with changing rainfall patterns in the Congo Basin after 2.2 kyr BP, could be responsible, at least locally, for accelerated soil erosion and more intense chemical weathering. This series of events would provide a complementary mechanism possibly accounting for the magnitude of the environmental disturbances that took place in Central Africa during the late Holocene, suggesting that after an initial climatic trigger land-use intensification also played a role in the rainforest crisis.

5. Concluding remarks

This study provides evidence for a major landscape reorganization in the Congo Basin from ca. 2.2 kyr BP onward, associated with forest retreat and expansion of savannas. This event occurred contemporaneously with a period of climate instability and was characterized by erosion of pre-aged and intensively weathered soils, which could indicate remobilization of swamp deposits from the central part of the watershed, in response to decreased water levels in the Cuvette Centrale. We propose that changing hydroclimate patterns in the Congo Basin at that time were triggered by the onset of enhanced ENSO variability, possibly leading to opening of human dispersal routes towards the east and favoring the migration of Bantu-speaking populations across Central Africa. While it remains difficult to discriminate between climate and human activities as the dominant cause of abrupt environmental changes in the vast Congo basin, it is very likely that these factors were closely interconnected during the late Holocene rainforest crisis.

Acknowledgements

This work was funded via an IEF Marie Curie fellowship to G.B. (Grant No. FP7-PEOPLE-2012-IEF 327778) and the DFG Research Center/Cluster of Excellence “The Ocean in the Earth System” at MARUM. We are very grateful to S. Bouillon for providing bulk organic data and important feedback on this work. We also thank J. Etoubleau for major element analyses, the participants of the ZAIROV cruise (PI: Bruno Savoye) for their assistance at sea, and C. Delvaux for providing sediment from Lake Kivu. The Editor (D. Vance) and three anonymous reviewers are also greatly acknowledged for providing constructive comments on this manuscript. The TransCongo project was funded through a FNRS grant (PDR 14711103) and a European Research Council Starting Grant (ERC-StG 240002 AFRIVAL). All data reported in this paper are listed in the Supplementary Material.

Appendix A. Supplementary material

Supplementary material related to this article can be found online at https://doi.org/10.1016/j.epsl.2018.10.016.

References

Allègre, C.J., Dupré, B., Negrel, P., Gaillardet, J., 1996. Sr–Nd–Pb isotope systematics in Amazon and Congo River systems: constraints about erosion processes. Chem. Geol. 131, 93–112.

Babonneau, N., Savoye, B., Cremer, M., Bez, M., 2004. Multiple terraces within the deep incised Zaire Valley (ZaïAngo Project): are they confined levees? Geol. Soc. (Lond.) Spec. Publ. 222, 91–114.

Bayon, G., German, C.R., Boella, R.M., Milton, J.A., Taylor, R.N., Nesbitt, R.W., 2002. Sr and Nd isotope analyses in paleoceanography: the separation of both detrital and Fe–Mn fractions from marine sediments by sequential leaching. Chem. Geol. 187, 179–199.

Bayon, G., Burton, K.W., Soulet, G., Vigier, N., Dennielou, B., Etoubleau, J., Ponzevera, E., German, C.R., Nesbitt, R.W., 2009. Hf and Nd isotopes in marine sediments: constraints on global silicate weathering. Earth Planet. Sci. Lett. 277, 318–326.

Bayon, G., Dennielou, B., Etoubleau, J., Ponzevera, E., Toucanne, S., Bermell, S., 2012. Intensifying weathering and land use in Iron Age Central Africa. Science 335, 1219–1222.

Bayon, G., Toucanne, S., Skonieczny, C., André, L., Bermell, S., Cheron, S., Dennielou, B., Etoubleau, J., Freslon, N., Gauchery, T., Germain, Y., Jorry, S.J., Ménot, G., Monin, L., Ponzevera, E., Rouget, M.-L., Tachikawa, K., Barrat, J.A., 2015. Rare Earth elements and neodymium isotopes in world river sediments revisited. Geochim. Cosmochim. Acta 170, 17–38.

Bayon, G., Delvigne, C., Ponzevera, E., Borges, A.V., Darchambeau, F., De Deckker, P., Lambert, T., Monin, L., Toucanne, S., André, L., 2018. The silicon isotopic composition of fine-grained river sediments and its relation to climate and lithology. Geochim. Cosmochim. Acta 229, 147–161.

Borges, A.V., Darchambeau, F., Teodoru, C.R., Marwick, T.R., Tamooh, F., Geeraert, N., Omengo, F.O., Guérin, F., Lambert, T., Morana, C., Okuku, E., Bouillon, S., 2015. Globally significant greenhouse gas emissions from African inland waters. Nat. Geosci. 8, 637–642.

Bostoen, et al., 2015. Middle to late Holocene paleoclimatic change and the early Bantu expansion in the rain forests of Western Central Africa. Curr. Anthropol. 56, 354–384.

Bouchez, J., Gaillardet, J., France-Lanord, C., Maurice, L., Dutra-Maia, P., 2011. Grain size control of river suspended sediment geochemistry: clues from Amazon River depth profiles. Geochem. Geophys. Geosyst. 12 (3).

Bouvier, A., Vervoort, J.D., Patchett, P.J., 2008. The Lu–Hf and Sm–Nd isotopic composition of CHUR: constraints from unequilibrated chondrites and implications for the bulk composition of terrestrial planets. Earth Planet. Sci. Lett. 273, 48–57.
Conroy, J.L., Overpeck, J.T., Cole, J.E., Shanahan, T.M., Steinitz-Kannan, M., 2008. Holocene changes in eastern tropical Pacific climate inferred from a Galápagos lake sediment record. Quat. Sci. Rev. 27, 1166–1180.
Dalibard, M., Popescu, S.M., Maley, J., Baudin, F., Melinte-Dobrinescu, M.C., Pittet, B., Marsset, T., Dennielou, B., Droz, L., Suc, J.P., 2014. High-resolution vegetation history of West Africa during the last 145 ka. Geobios 47, 183–198.
Dargie, G.C., Lewis, S.L., Lawson, I.T., Mitchard, E.T.A., Page, S.E., Bocko, Y.E., Ifo, S.A., 2017. Age, extent and carbon storage of the central Congo Basin peatland complex. Nature 542, 86–90.
Diamond, J., Bellwood, P., 2003. Farmers and their languages: the first expansions. Science 300, 597–603.
Foerster, V., et al., 2012. Climatic change recorded in the sediments of the Chew Bahir basin, southern Ethiopia, during the last 45,000 years. Quat. Int. 274, 25–37.
Garcin, Y., et al., 2018. Early anthropogenic impact on Western Central African rainforests 2,600 y ago. Proc. Natl. Acad. Sci. USA. https://doi.org/10.1073/pnas.1715336115.
Gomez, B., Carter, L., Orpin, A.R., Cobb, K.M., Page, M.J., Trustrum, N.A., Palmer, A.S., 2012. ENSO/SAM interactions during the middle and late Holocene. Holocene 22, 23–30.
Govin, A., Holzwarth, U., Heslop, D., Ford Keeling, L., Zabel, M., Mulitza, S., Collins, J.A., Chiessi, C.M., 2012. Distribution of major elements in Atlantic surface sediments (36 N–49 S): imprint of terrigenous input and continental weathering. Geochem. Geophys. Geosyst. 13 (1).
Grollemund, R., Branford, S., Bostoen, K., Meade, A., Venditti, C., Page, P., 2015. Bantu expansion shows that habitat alters the route and pace of human dispersals. Proc. Natl. Acad. Sci. USA 112, 13296–13301.
Hemingway, J.D., Schefuß, E., Spencer, R.G.M., Dinga, B.J., Eglinton, T.I., McIntyre, C., Galy, V.V., 2017. Hydrologic controls on seasonal and inter-annual variability of Congo River particulate organic matter source and reservoir age. Chem. Geol. 466, 454–465.
Hopmans, E.C., Weijers, J.W.H., Schefuß, E., Herfort, L., Sinninghe Damsté, J.S., Schouten, S., 2004. A novel proxy for terrestrial organic matter in sediments based on branched and isoprenoid tetraether lipids. Earth Planet. Sci. Lett. 224, 107–116.
Ivory, S.J., McGlue, M.M., Ellis, G.S., Boehlke, A., Lézine, A.M., Vincens, A., Cohen, A.S., 2017. East African weathering dynamics controlled by vegetation-climate feedbacks. Geology 45, 823–826.
Junginger, A., Roller, S., Olaka, L.A., Trauth, M.H., 2014. The effects of solar irradiation changes on the migration of the Congo Air Boundary and water levels of paleo-Lake Suguta, Northern Kenya Rift, during the African Humid Period (15–5 ka BP). Palaeogeogr. Palaeoclimatol. Palaeoecol. 396, 1–16.
Lambert, T., Bouillon, S., Darchambeau, F., Massicotte, P., Borges, A.V., 2016. Shift in the chemical composition of dissolved organic matter in the Congo River network. Biogeosciences 13, 5405–5420.
Laraque, A., Bricquet, J.P., Pandi, A., Olivry, J.C., 2009. A review of material transport by the Congo River and its tributaries. Hydrol. Process. 23, 3216–3224.
Laraque, A., Castellanos, B., Steiger, J., Lòpez, J.L., Pandi, A., Rodriguez, M., Rosales, J., Adèle, G., Perez, J., Lagane, C., 2013. A comparison of the suspended and dissolved matter dynamics of two large inter-tropical rivers draining into the Atlantic Ocean: the Congo and the Orinoco. Hydrol. Process. 27, 2153–2170.
Lézine, A.M., Holl, A.F.C., Lebamba, J., Vincens, A., Assi-Khaudjis, C., Février, L., Sultan, E., 2013. Temporal relationship between Holocene human occupation and vegetation change along the northwestern margin of the Central African rainforest. C. R. Geosci. 345, 327–335.
Lu, Z., Liu, Z., Zhu, J., Cobb, K.M., 2018. A review of paleo El Niño-Southern Oscillation. Atmosphere 9, 130.
Lupo, K.D., Schmitt, D.N., Kiahtipes, C.A., Ndanga, J.P., Young, D.C., Simiti, B., 2015. On intensive late Holocene Iron mining and production in the Northern Congo Basin and the environmental consequences associated with metallurgy in Central Africa. PLoS ONE. https://doi.org/10.1371/journal.pone.0132632.
Macreadie, P.I., Rolph, T.C., Boyd, R., Schröder-Adams, C.J., Skilbeck, C.G., 2015. Do ENSO and coastal development enhance coastal burial of terrestrial carbon? PLoS ONE 10, 0145136.
Maher Jr., L.J., 1972. Nomograms for computing 0.95 confidence limits of pollen data. Rev. Palaeobot. Palynol. 13, 85–93.
Maley, J., 2001. *Elaeis guineensis* Jacq. (oil palm) fluctuations in central Africa during the late Holocene: climate or human driving forces for this pioneering species? Veg. Hist. Archaeobot. 10, 117–120.
Maley, J., 2002. A catastrophic destruction of African forests about 2,500 years ago still exerts a major influence on present vegetation formations. IDS Bull. 33, 13–30.
Maley, J., Giresse, P., Doumengue, C., Favier, C., 2012. Comment on "Intensifying weathering and land use in Iron Age Central Africa". Science 337, 1040.
Maley, J., Doumenge, C., Giresse, P., Mahé, G., Philippon, N., Hubau, W., Lokonda, M.O., Tshibamba, J.M., Chepstow-Lusty, A., 2018. Late Holocene forest contraction and fragmentation in central Africa. Quat. Res. 89, 43–59.
Mbuebue, J.M.T., Muliwavyo, A.M., Mwamba, V.L., Phuati, E.P., Bantu, A.K.M., Keto, F.T., 2016. Time-scale characteristics of Kasai river hydrological regime variability for 1940–1999. arXiv:1611.07317.
Morin-Rivat, J., Fayolle, A., Gillet, J.F., Bourland, N., Gourlet-Fleury, S., Oslisly, R., Bremond, L., Bentaleb, I., Beeckman, H., Doucet, J.L., 2014. New evidence of human activities during the Holocene in the lowland forests of the northern Congo basin. Radiocarbon 56, 209–220.
Neumann, K., et al., 2012. Comment on "Intensifying weathering and land use in Iron Age Central Africa". Science 337, 1040.
Ngomanda, A., Neumann, K., Schweizer, A., Maley, J., 2009. Seasonality change and the third millennium BP rainforest crisis in southern Cameroon (Central Africa). Quat. Res. 71, 307–318.
Nicholson, S.E., Kim, J., 1997. The relationship of the El Niño-Southern Oscillation to African rainfall. Int. J. Climatol. 17, 117–135.
Oslisly, R., White, L., Bentaleb, I., Favier, C., Fontugne, M., Gillet, J.F., Sebag, D., 2013. Climatic and cultural changes in the West Congo basin forests over the past 5000 years. Philos. Trans. R. Soc. Lond. B, Biol. Sci. 368, 20120304.
Phillipson, D.W., 2005. African Archaeology, 3rd edition. Cambridge University Press, Cambridge.
Preethi, B., Sabin, T.P., Adedoyin, J.A., Ashok, K., 2015. Impacts of the ENSO Modoki and other tropical Indo-Pacific climate-drivers on African Rainfall. Sci. Rep. 5. https://doi.org/10.1038/srep16653.
Ropelewski, C.F., Halpert, M.S., 1987. Global and regional scale precipitation patterns associated with the El Niño/Southern Oscillation. Mon. Weather Rev. 115, 1606–1626.
Sachse, D., et al., 2012. Molecular paleohydrology: interpreting the hydrogen-isotopic composition of lipid biomarkers from photosynthesizing organisms. Annu. Rev. Earth Planet. Sci. 40, 221–249.
Schefuß, E., Schouten, S., Schneider, R.R., 2005. Climatic controls on central African hydrology during the past 20,000 years. Nature 437, 1003–1006.
Schefuß, E., Eglinton, T.I., Spencer-Jones, C.L., Rullkötter, J., De Pol-Holz, R., Talbot, H.M., Grootes, P.M., Schneider, R.R., 2016. Hydrologic control of carbon cycling and aged carbon discharge in the Congo River basin. Nat. Geosci. 9, 687–690.
Schneider, R.R., Price, B., Muller, P., Kroon, D., Alexander, I., 1997. Monsoon-related variations in Zaire (Congo) sediment load and influence of fluvial silicate supply on marine productivity in the east equatorial Atlantic during the last 200,000 years. Paleoceanography 12, 463–481.
Singarayer, J.S., Burrough, S.L., 2015. Interhemispheric dynamics of the African rainbelt during the late Quaternary. Quat. Sci. Rev. 124, 48–67.
Sowunmi, M.A., 1999. The significance of the oil palm (*Elaeis guineensis* Jacq.) in the late Holocene environments of west and west central Africa: a further consideration. Veg. Hist. Archaeobot. 8, 199–210.
Stuiver, M., Polach, H.A., 1977. Discussion reporting of ^{14}C data. Radiocarbon 19, 355–363.
Stuiver, M., Reimer, P.J., Reimer, R.W., 2017. CALIB 7.1. http://calib.qub.ac.uk/calib/.
Tanaka, T., et al., 2000. JNdi-1: a neodymium isotopic reference in consistency with LaJolla neodymium. Chem. Geol. 168, 179–181.
Thiéblemont, D., Flehoc, C., Ebang-Obiang, M., Rigollet, C., Prian, J.P., Prognon, F., 2013. Geochronological arguments for a close relationship between surficial formation profiles and environmental crisis (c. 3000–2000 BP) in Gabon (Central Africa). C. R. Geosci. 345, 272–283.
Thiéblemont, D., Guerrot, C., Négrel, P., Braucher, R., Bourlès, D.L., Thieblemont, R., 2014. Nd-isotope evidence for the distal provenance of the historical (c. < 3000 BP) lateritic surface cover underlying the Equatorial forest in Gabon (Western Africa). Aeol. Res. 15, 177–192.
Tierney, J.E., Russell, J.M., Sinninghe Damsté, J.S., Huang, Y., Verschuren, D., 2011. Late Quaternary behavior of the East African monsoon and the importance of the Congo Air Boundary. Q. Sci. Res. 30, 798–807.
Vincens, A., et al., 1998. Biome reconstruction from pollen and plant macrofossil data for Africa and the Arabian peninsula at 0 and 6000 years. J. Biogeogr. 25, 1007–1027.
Vincens, A., Lézine, A.M., Buchet, G., Lewden, D., Le Thomas, A., 2007. African pollen database inventory of tree and shrub pollen types. Rev. Palaeobot. Palynol. 145, 135–141.
Willis, K.J., Gillson, L., Brncic, T.M., 2004. How "virgin" is virgin rainforest? Science 304, 402–403.
Winterfeld, M., Mollenhauer, G., Dummann, W., Köhler, P., Lembke-Jene, L., Meyer, V.D., Hefter, J., McIntyre, C., Wacker, L., Kokfelt, U., Tiedemann, R., 2018. Deglacial mobilization of pre-aged terrestrial carbon from degrading permafrost. Nat. Commun. 9, 3666.